Effect of High Voltage on the Structure and Electrochemistry of $LiNi_{0.5}Mn_{0.5}O_2$: A Joint Experimental and Theoretical Study

Julien Bréger,[†] Ying S. Meng,[‡] Yoyo Hinuma,[‡] Sundeep Kumar,[§] Kisuk Kang,[‡] Yang Shao-Horn,[§] Gerbrand Ceder,[‡] and Clare P. Grey*,[†]

Department of Chemistry, State University of New York at Stony Brook, Stony Brook, New York 11794, and Department of Materials Science and Engineering and Department of Mechanical Engineering, Massachusetts Institute of Technology, Cambridge, Massachusetts 02139

Received April 17, 2006. Revised Manuscript Received July 13, 2006

A combination of neutron diffraction (ND), ^{6}Li magic-angle spinning NMR, electrochemistry, and first principles calculations have been used to determine and rationalize the structural changes that occur during cycling of the layered material $Li_x(Ni_{0.5}Mn_{0.5})O_2$ ($x = 1$), synthesized via the hydroxide route. ND and ^{6}Li NMR experiments confirm that Li is lost from the transition metal (TM) layers, very early on in the charge process. On charging to higher voltages (above 4.5 V), the Li is lost from the tetrahedral and residual Li octahedral sites in the Li layers. This process is accompanied by a migration of more than 75% of the Ni ions originally present in the Li layers into the TM layers, to occupy the sites vacated by Li. Calculations suggest that (i) these Ni migrations occur via the tetrahedral sites, (ii) activation energies for migration depend strongly on the original position of the Ni ions in the Li layers though the driving force for migration is large (>1 eV), and (iii) because neither Ni^{3+} nor Ni^{4+} is stable in the tetrahedral site, migration will not occur once the Ni ions in the Li layers are oxidized to Ni^{3+} or Ni^{4+}. Electrochemical measurements (open circuit voltage, OCV, and galvanostatic mode) are consistent with a high voltage process (approximately 4.6 V) associated with a large activation energy. The new Ni sites in the TM layers are not necessarily stable, and on discharge, 60% of the ions return to the Li layers. In particular, Ni ions surrounded by six Mn^{4+} ions are found (in the calculations) to be the least stable. Because the Li ions originally in the TM layers in the as-synthesized sample are predominantly in this environment, this is consistent with the Ni migration observed experimentally. Materials charged to 5.3 V can be cycled reversibly with stable capacities of over 180 mAh g^{-1}.

Introduction

Layered lithium nickel manganese oxides are promising, inexpensive, and nontoxic alternative positive electrode materials to the commercial $LiCoO_2$ electrode used in Li-ion batteries. Among these materials, $LiNi_{0.5}Mn_{0.5}O_2$ is particularly attractive because of its high theoretical capacity (280 mAh g^{-1}). Its electrochemical and structural properties have, therefore, been thoroughly investigated over the past few years.[1−3] The Ni^{2+} ions are electrochemically active, the Mn ions remaining as Mn^{4+} throughout the cycling process.[4−7] $LiNi_{0.5}Mn_{0.5}O_2$ adopts the layered α-$NaFeO_2$ structure (space group $R\bar{3}m$, Figure 1a),[8] but a considerable amount of Li and Ni is exchanged between the Li(3a) and Ni/Mn(3b) layers due to the similar size of the Li^+ and Ni^{2+} cations. Two compositional strategies exist for reducing the Ni content in the Li layer and increasing the layered character of the structure. (1) The first involves moving toward the Li_2MnO_3 composition by substituting three Ni for two Li and one Mn, thereby reducing the theoretical capacity of the material. These compositions $Li(Li_{1/3-2x/3}Ni_xMn_{2/3-x/3})O_2$ have been extensively investigated.[9−11] (2) The second involves substituting some Ni and Mn for Co ions, which increases the layering of the material,[12−13] but this time at the expense of thermal stability.[14] As the central starting point for these compositional modifications, $LiNi_{0.5}Mn_{0.5}O_2$ has the largest theoretical energy density and provides good thermal stability and a very high energy density at low rate. Recently, it was

* To whom correspondence should be addressed. E-mail: cgrey@notes.cc.sunysb.edu.
[†] State University of New York at Stony Brook
[‡] Department of Materials Science and Engineering, Massachusetts Institute of Technology.
[§] Department of Mechanical Engineering, Massachusetts Institute of Technology.

(1) Ohzuku, T.; Makimura, Y. *Chem. Lett.* **2001**, 744.
(2) Makimura, Y.; Ohzuku, T. *J. Power Sources* **2003**, *119*−*121*, 156.
(3) Lu, Z.; MacNeil, D. D.; Dahn, J. R. *Electrochem. Solid-State Lett.* **2001**, *4*, A191.
(4) Yoon, W.-S.; Grey, C. P.; Balasubramanian, M.; Yang, X.-Q.; McBreen, J. *Chem. Mater.* **2003**, *15*, 3161.
(5) Kobayashi, H.; Sakaebe, H.; Kageyma, H.; Tatsumi, K.; Arachi, Y.; Kamiyama, T. *J. Mater. Chem.* **2003**, *13*, 590.
(6) Johnson, C. S.; Kim, J.-S.; Kropf, A. J.; Kahaian, A. J.; Vaughey, J. T.; Fransson, L. M. L.; Edström, K.; Thackeray, M. M. *Chem. Mater.* **2003**, *15*, 2313.
(7) Reed, J.; Ceder, G. *Electrochem. Solid-State Lett.* **2002**, *5*, A145.
(8) Mizushima, K.; Jones, P. C.; Wiseman, P. J.; Goodenough, J. B. *Mater. Res. Bull.* **1980**, *15*, 783.
(9) Lu, Z.; Dahn, J. R. *J. Electrochem. Soc.* **2002**, *149*, A815.
(10) Lu, Z.; Beaulieu, L. Y.; Donaberger, R. A.; Thomas, C. L.; Dahn, J. R. *J. Electrochem. Soc.* **2002**, *149*, A778.
(11) Kim, J.-S.; Johnson, C. S.; Vaughey, J. T.; Thackeray, M. M. *Chem. Mater.* **2004**, *16*, 1996.
(12) Lu, Z.; MacNeil, D. D.; Dahn, J. R. *Electrochem. Solid-State Lett.* **2001**, *4*, A200.
(13) Ohzuku, T.; Makimura, Y. *Chem. Lett.* **2001**, 642.
(14) Jiang, J.; Eberman, K. W.; Krause, L. J.; Dahn, J. R. *J. Electrochem. Soc.* **2005**, *152*, A1879.

10.1021/cm060886r CCC: $33.50
Published on Web 08/31/2006

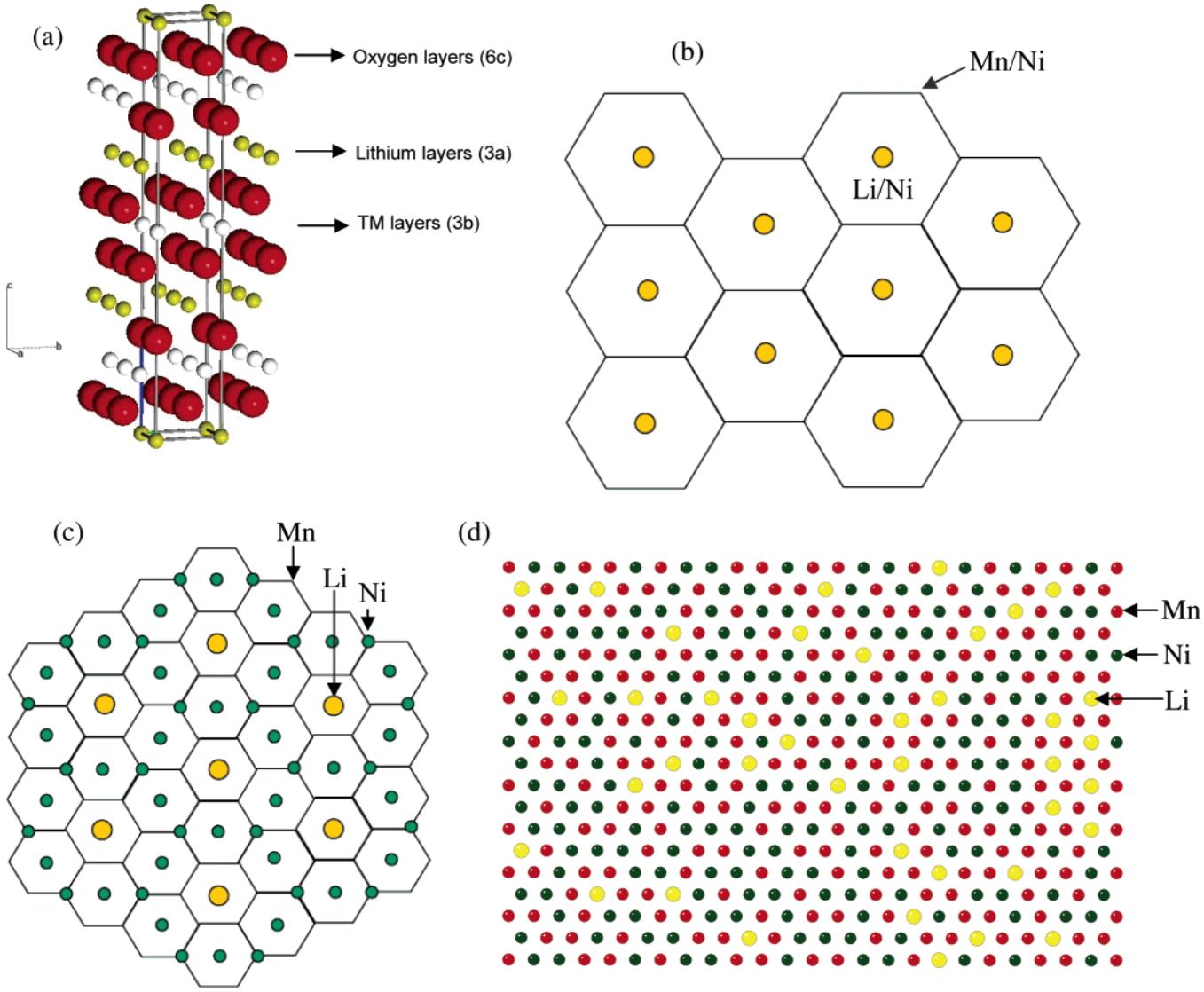

Figure 1. (a) Ideal structural model of $LiNi_{0.5}Mn_{0.5}O_2$.[8] Ni and Mn atoms share the 3b sites. (b−d) Different models for ordering of the cations in the TM layers. (b) Honeycomb ordering for a TM layer with composition $[Li_{0.1}Mn_{0.5}Ni_{0.4}]$; the structure is derived from the Li_2MnO_3 structure, by replacing three Ni^{2+} ions for two Li^+ and 1 Mn^{4+} ions, to maintain charge balance in the layers. Each Li or Ni atom (in yellow) in the TM layers is surrounded by six Mn or Ni atoms at the corners of the hexagons. (c) The flower-like ordering predicted by first-principles calculations, with a composition of $[Li_{0.08}Mn_{0.5}Ni_{0.42}]$ for the layer. The Li, Ni, and Mn atoms are in yellow and green and at the empty corners of the hexagons, respectively.[20] (d) A representative snapshot of the cation arrangements obtained in recent MC simulations at 1000 K. The Li, Ni, and Mn atoms are in yellow, green, and red, respectively.

further shown that a more layered version of $LiNi_{0.5}Mn_{0.5}O_2$ can rival the rate capability of the Co-substituted materials.[15] The objective of this work is to investigate in detail the delithiation process of $LiNi_{0.5}Mn_{0.5}O_2$ and characterize any changes in the transition metal (TM) configuration that take place upon cycling.

The Li/Ni disorder in samples synthesized by regular solid-state routes plays a central role in determining the structure of $LiNi_{0.5}Mn_{0.5}O_2$. Li magic-angle spinning (MAS) NMR experiments found Li^+ ions in the TM layers of $LiNi_{0.5}Mn_{0.5}O_2$, surrounded predominantly by five to six Mn^{4+} ions resembling the environment in Li_2MnO_3,[16,17] while X-ray and neutron diffraction (ND) studies by Lu et al.[3,9,10] indicated partial exchange (8−10% of the Ni ions) between the Ni and the Li ions in the TM and Li layers. The low energy of the $LiMn_6$ honeycomb motif present in Li_2MnO_3 was suggested to provide a driving force for the Li^+/Ni^{2+} exchange.[16,17] More recently, we used a combination of NMR and pair distribution function analysis of ND data to investigate both Li and TM local ordering.[18] The results were analyzed by considering three structural models, (I) random distributions of the Li, Ni, and Mn cations in the TM layers, (II) a honeycomb model in which the triangular lattice of the TM layer is separated into a Li-rich sublattice and a Mn-rich sublattice (Figure 1b), and (III) a more complex flower-like ordering[19] (Figure 1c) whereby $LiMn_6$ rings are surrounded by larger Ni rings. The combined NMR and neutron data provided strong evidence for a nonrandom distribution

(15) Kang, K.; Meng, Y. S.; Bréger, J.; Grey, C. P.; Ceder, G. *Science* **2006**, *311*, 977.
(16) Yoon, W.-S.; Paik, Y.; Yang, X.-Q.; Balasubramanian, M.; McBreen, J.; Grey, C. P. *Electrochem. Solid-State Lett.* **2002**, *5*, A263.
(17) Yoon, W.-S.; Iannopollo, S.; Grey, C. P.; Carlier, D.; Gorman, J.; Reed, J.; Ceder, G. *Electrochem. Solid-State Lett.* **2004**, *7*, A167.
(18) Bréger, J.; Dupré, N.; Chupas, P. J.; Lee, P. L.; Proffen, T.; Parise, J. B.; Grey, C. P. *J. Am. Chem. Soc.* **2005**, *127*, 7529.
(19) Van der Ven, A.; Ceder, G. *Electrochem. Commun.* **2004**, *6*, 1045.

of the cations, with much stronger Li−Ni avoidance than predicted by simple honeycomb ordering, the resulting structure more resembling a partially disordered "flower" arrangement. Recent Monte Carlo (MC) simulations by Hinuma et al.[20] (Figure 1d) are in very good agreement with this model, indicating that materials produced via high-temperature routes show considerable disorder over that predicted from ground-state structures but still retain some of the key structural features of the flower ordering, namely, Li−Ni avoidance.

While these previous studies have improved our understanding of the pristine structure, less clarity exists as to the structural changes that occur upon delithiation of the material. Makimura[21] has shown that the deintercalated material $Li_xNi_{0.5}Mn_{0.5}O_2$, $x < 1$, maintains the parent hexagonal $R\bar{3}m$ cell throughout, while Arachi et al. have observed a transition from the hexagonal $R\bar{3}m$ cell to a monoclinic $C2/m$ cell between $x = 0.7$ and $x = 0.8$.[22] These authors also found that a fraction of the octahedral Li and Ni atoms migrate to tetrahedral sites upon charge.[22,23] Previous ex situ NMR experiments on charged samples have shown that the structural changes are even more complex. The Li located in the TM layers is removed very early on in the charge process:[16] approximately 50% of these ions have left the TM layers for $x = 0.7$, and they have essentially all disappeared for $x = 0.4$.[16] These results are in qualitative agreements with predictions from first principles calculations made for the perfect flower structure, which show that the Li ions migrate into the tetrahedral sites that share faces with the vacated octahedral site in the TM layers very early on in the charge process.[19] The occupation of tetrahedral sites is an obvious consequence of the Li extraction from the TM layer. While in a perfectly layered material, all tetrahedral sites share at least one face with the octahedral cation in the TM layers, a vacancy in the TM layer creates two empty tetrahedral sites in the Li layers above and below the TM layer. Both these sites can be occupied by Li, creating Li dumbbells if no nearest neighbor tetrahedral sites are already occupied (Figure 2).

Despite much work on this system, a number of issues, which are pivotal to the understanding of the functioning of these electrode materials, are poorly understood. For example, while the first principles calculations predict that there may be a high voltage process involving removal of the tetrahedral Li ions[19] and the diffraction results suggest that Ni may not always remain in its original site,[22] the details of why and when the Ni ions move are not known. Furthermore, our recent results, on a layered material with essentially no Li/Ni exchange and excellent high rate performance, shows that the Ni populations in the Li layers play a key role in controlling the slab spacing and, hence, the Li-ion conductivity in the Li layers.[15] The aim of the work presented in this paper is to combine results from neutron and X-ray diffraction (XRD), ^{6}Li MAS NMR spectroscopy, and calculations to determine and then rationalize the structural changes that occur on charging $Li_xNi_{0.5}Mn_{0.5}O_2$. The effect of charging to high voltages, to establish whether the tetrahedral Li ions can indeed be removed, and the consequent effect of this on the structure are explored.

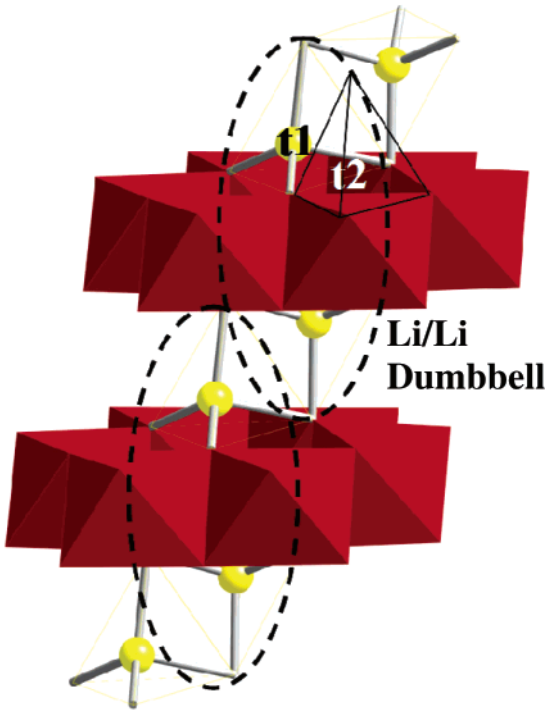

Figure 2. Li−Li dumbbell formed from a Li vacancy in the TM layers (Li_{TM}^{V}) and two adjacent tetrahedral Li ions t1 above and below the TM layer. Li−Ni dumbbells are formed from two adjacent tetrahedral Ni and Li ions. t2 is the tetrahedral site adjacent to the t1 site in the same plane.

Materials and Methods

Sample Preparation. $LiNi_{0.5}Mn_{0.5}O_2$ powders were prepared by the mixed hydroxide method.[3] A 50 mL aqueous solution of stoichiometric amounts of TM nitrates was prepared and slowly dripped (1−2 h) into 400 mL of a stirred solution of LiOH using a burette, yielding a precipitation of $M(OH)_2$, where M = Mn and Ni, with a homogeneous cation distribution. The dried precipitate was mixed with $Li(OH)\cdot H_2O$ in stoichiometric proportions. The mixture was then heated in air at 480 °C for 12 h, annealed at 900 °C or 1000 °C for another 12 h, and quenched between two copper plates. The samples were prepared with $^6Li(OH)\cdot H_2O$ (Cambridge Isotopes, 90−95%) for ^{6}Li MAS NMR measurements to maximize the signal/noise ratio and acquisition time and with $^7Li(OH)\cdot H_2O$ (Aldrich, >97%) for ND experiments to minimize absorption from the ^{6}Li nuclei.

Electrochemistry. For the ^{6}Li MAS NMR experiments, synchrotron XRD, and cycling experiments, cathodes were prepared by mixing 80 wt % of active material ($^6LiNi_{0.5}Mn_{0.5}O_2$), 10 wt % of acetylene black as an electronic conductor, and 10 wt % of poly(vinylidene fluoride) binder in *N*-methyl pyrrolidone (NMP). The slurry was deposited on an aluminum foil and dried at 80 °C until the solvent had evaporated completely. Coin cells (CR2032, Hohsen Corp.) were assembled in an argon-filled glove box. Each cell contains typically about 15 mg of active material, separated from a Li foil (^{6}Li foil was when preparing the NMR samples) by two pieces of Celgard separator (Celgard, Inc., U.S.A.). A 1 M solution of $LiPF_6$ in ethylene carbonate/dimethyl carbonate (1:1) has been

(20) Hinuma, Y.; Meng, Y. S.; Kisuk, K.; Ceder, G. To be published.
(21) Makimura, Y. Ph.D. Thesis, Osaka City University, 2003.
(22) Arachi, Y.; Koabayashi, H.; Emura, S.; Nakata, Y.; Tanaka, M.; Asai, T.; Sakaebe, H; Tatsumi, K.; Kageyama, H. *Solid State Ionics* **2005**, *176*, 895.
(23) Kobayashi, H.; Arachi, Y.; Kageyama, H.; Tatsumi, K. *J. Mater. Chem.* **2004**, *14*, 40.

used as the electrolyte. Electrochemical experiments were carried out on a battery cycler (Arbin Instruments, College Station, TX) in galvanostatic mode at a *C*/20 rate.

Slightly different electrode mixtures were used to prepare cycled samples suitable for the ND experiments, to reduce the total proton content of these electrodes, to minimize absorption problems. A 300 mg mixture containing 90% of active material ($^7LiNi_{0.5}Mn_{0.5}O_2$) and 10% of graphite (Timrex KS44) was deposited on an aluminum plate and dried at 80 °C until complete evaporation of NMP; no binder was used. Swagelok-type cells were assembled in an argon-filled glove box. They were separated from a lithium foil by two sheets of fiberglass filters. The whole assembly was soaked in the electrolyte, an ethylene carbonate/dimethyl carbonate (1:1) solution of $LiPF_6$ (1 M). Electrochemical experiments were carried out at a *C*/200 rate. The samples were washed with deuterated acetone before ND experiments, again to reduce proton contents in the samples. Some of these samples were analyzed by inductively coupled plasma−optical emission spectroscopy (ICP-OES) by Galbraith, to compare the Li contents with those estimated from the electrochemical data.

ND. ND experiments were performed on the General Materials Diffractometer (GEM) instrument at ISIS (Didcot, U.K.), on the General Purpose Powder Diffractometer (GPPD) instrument at the Intense Pulse Neutron Source (IPNS, Argonne National Laboratory), and on the Neutron Powder Diffractometer (NPDF) instrument at the Los Alamos Neutron Science Center (LANSCE, Los Alamos National Laboratory). The samples (from 300 mg to 1 g) were packed into 0.25 in. inside diameter thin-walled vanadium cans in a helium-filled glovebox.

In Situ XRD Diffraction. Experiments were performed at beamline X7A at the National Synchrotron Light Source (NSLS) located at Brookhaven National Laboratory, using a cell design identical to that described elsewhere.[24] Synchrotron radiation with a wavelength of 0.6482 Å and a step size of 0.25° every 5 s were employed.

MAS NMR Spectroscopy. The ^{6}Li MAS NMR experiments were performed with a double-resonance 2 mm probe, built by Samoson and co-workers,[25] on a CMX-200 spectrometer using a magnetic field of 4.7 T. The spectra were collected at an operating frequency of 29.46 MHz. A spinning frequency between 35 and 40 kHz and a rotor-synchronized spin−echo sequence ($90°-\tau-180°-\tau-$acq) were used to acquire the spectra. $\pi/2$ pulses of 3.5 μs were used, with recycle delay times of 0.2 s. All the NMR spectra were referenced to a 1 M ^{6}LiCl solution, at 0 ppm, and were scaled according to the acquisition number and the sample weight in the rotor.

Calculations Methodology. All energies are calculated with the spin-polarized generalized gradient approximation to density functional theory (DFT), using a plane-wave basis set and the projector-augmented wave method as implemented in the Vienna ab initio simulation package (VASP). A plane-wave basis with a kinetic energy cutoff of 370 eV was used. The reciprocal-space *k*-point grids between $3 \times 3 \times 3$ and $7 \times 7 \times 7$ were used depending on the size of the supercell considered. Structures were fully relaxed. The +U correction term in the Dudarev scheme[26] was used with $U = 5.96$ eV for Ni and $U = 5$ eV for Mn. This +U scheme corrects for the self-interaction in the TM *d* orbitals and has been shown to improve the prediction of voltages[27] and phase stability.[28] The local density approximation (LDA)+U approach was chosen for the *c*-lattice parameter calculation as it more accurately treats the Van der Waals interactions across the empty Li slab at the end of charge and has previously been shown to give qualitatively more correct variations in lattice parameter with Li concentration.[29]

Results and Analysis of the Experimental Data and Calculations

Electrochemistry. The potential (*V*) versus capacity (mAh g^{-1}) curve for $^6LiNi_{0.5}Mn_{0.5}O_2$ cycled five times between 4.6 and 2.0 V using a *C*/20 rate in galvanostatic mode (Figure 3a) shows electrochemical processes and capacities that are similar to those previously reported.[3] The irreversible capacity for the first cycle is around 15 mAh g^{-1}, similar to that reported by Lu et al.,[3] giving a stable capacity of 160 mAh g^{-1} in cycle 20 (Figure 3c). When cycled between 5.3 and 2.0 V, a new electrochemical process is observed, which is associated with a plateau above 5.0 V, leading to a capacity of 275 mAh g^{-1} (Figure 3b). This process is irreversible, and a stable capacity of over 180 mAh g^{-1} is achieved in the first 20 cycles, as shown in Figure 3d. This plateau (Figure 3b) is present for both electrodes constructed with acetylene black and graphite, where the latter were prepared for the ND experiments. Part of this additional capacity may result from the electrochemical intercalation of PF_6^- from the $LiPF_6$ electrolyte into the graphitic regions of the carbon and the associated reduction of Li^+ from the electrolyte at the anode, which was previously observed by Seel and Dahn to occur in this voltage window.[30] This process is only partially reversible. However, given the low carbon content of these electrodes, the capacity of the high voltage process is too large to account fully for the observed plateau (see Discussion and Supporting Information).

Very similar electrochemical data were obtained for the first charge for the larger cells used to prepare the ND samples. Cycling was arrested at selected potentials (4.1, 4.6, 4.8, and 5.2 V (charge) and 2.0 V (discharge)) to investigate the effect of the high voltage plateau on the electrode structure. The two samples cycled to either 4.8 or 5.2 V and then discharged to 2.0 V showed capacities of 233 and 265 mAh g^{-1} at the top of the charge, respectively, consistent with data in Figure 3. Only the 4.8 V charged sample showed unusual behavior, its Li content ($x = 0.4$; calculated using 100% Coulombic efficiency) being higher than that of the 4.6 V cell ($x = 0.33$). On the basis of the electrochemical data obtained in coin cells, the Li content of the 4.8 V cell is expected to be only slightly lower than that the 4.6 V sample ($x = 0.23$ (4.8 V) vs 0.33 (4.6 V)). Overall, the large cells used for ND experiments showed a much shorter discharge curve than that for the coin cells, which resulted in a smaller Li concentration (~0.6) at the end of discharge (see Supporting Information for the voltage curves).

The voltage profile of a $Li/Li_xNi_{0.5}Mn_{0.5}O_2$ cell with 6 h open circuit voltage (OCV) steps upon the first charge to

(24) Balasubramanian, M.; Sun, X.; Yang, X. Q.; McBreen, J. *J. Power Sources* **2001**, *92*, 1.
(25) Du, L.-S.; Samoson, A.; Tuherm, T.; Grey, C. P. *Chem. Mater.* **2000**, *12*, 3611.
(26) Dudarev, S. L.; Botton, G. A.; Savrasov, S. Y.; Humphreys, C. J.; Sutton, A. P. *Phys. Rev. B* **1998**, *57*, 1505.
(27) Zhou, F.; Cococcioni, M.; Marianetti, C. A.; Morgan, D.; Ceder, G. *Phys. Rev. B.* **2004**, *70*, 235121.
(28) Zhou, F.; Marianetti, C. A.; Cococcioni, M.; Morgan, D.; Ceder, G. *Phys. Rev. B* **2004**, *69*, 201101.
(29) Van der Ven, A.; Aydinol, M. K.; Ceder, G. *Phys. Rev. B* **1998**, *58*, 2975.
(30) Seel, J. A.; Dahn, J. R. *J. Electrochem. Soc.* **2000**, *147*, 892.

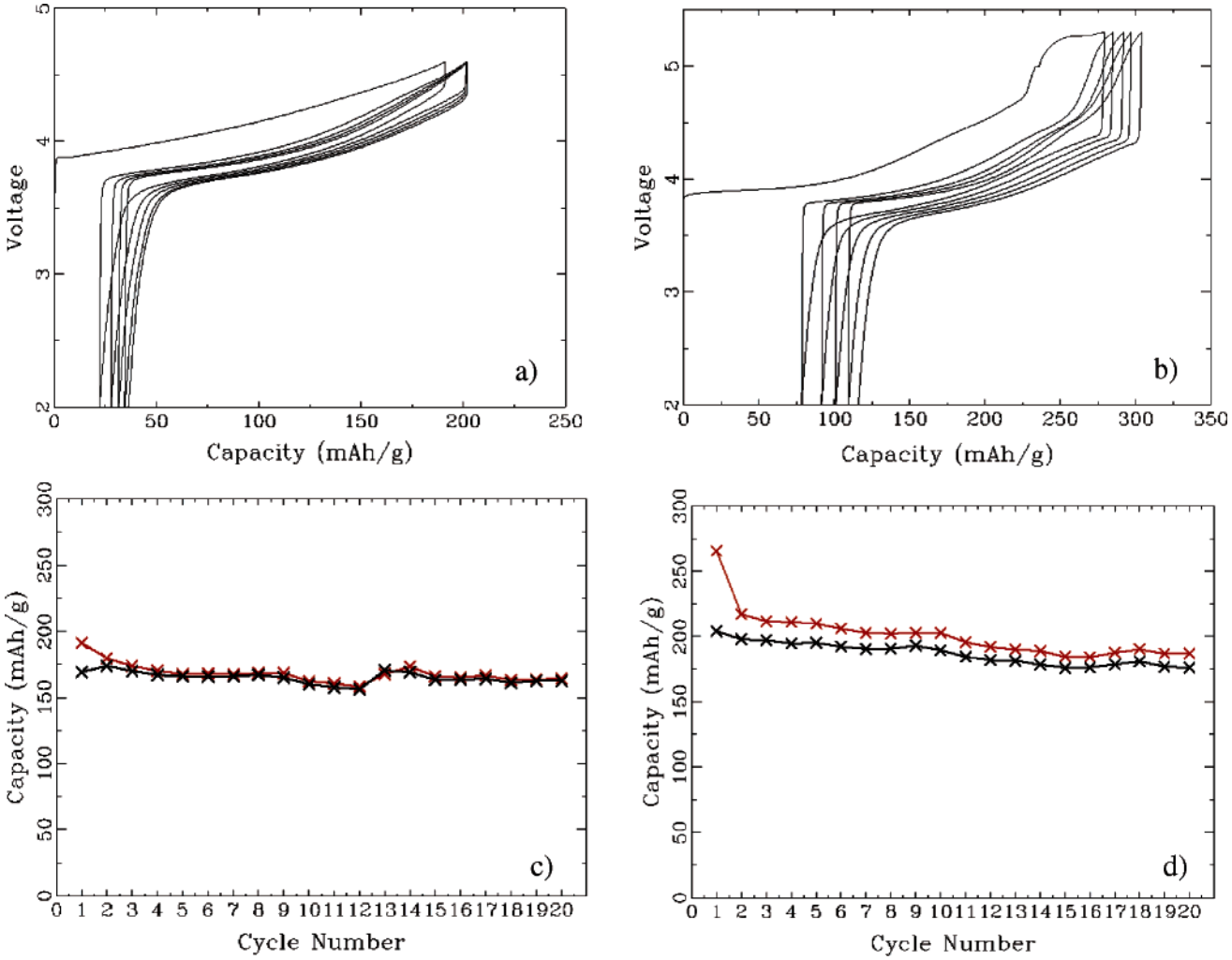

Figure 3. Voltage vs specific capacity curve for $^{6}LiNi_{0.5}Mn_{0.5}O_2$ cycled (five cycles) using a *C*/20 rate, in galvanostatic mode, (a) between 2.0 and 4.6 V and (b) between 2.0 and 5.3 V. The charge (red) and discharge (black) specific capacity as a function of cycle number for 20 cycles, (c) between 2.0 and 5.3 V and (d) between 2.0 and 4.6 V.

5.3 V under a current density corresponding to *C*/50 consists of two relatively flat regions at ~3.8 V and ~4.5 V and one sloping region in between. Notably, the OCV values flatten at 4.54 V at charging voltages higher than 4.90 V. This data is compared later with predictions from theory in Figure 9.

NMR. Figure 4a shows the ^{6}Li MAS NMR spectra of the $^{6}LiNi_{0.5}Mn_{0.5}O_2$ pristine material and samples charged to 4.8 and 5.3 V. The NMR samples, prepared in small electrochemical cells, have capacities that are essentially identical to those presented in Figure 3. The pristine spectrum is consistent with the work of Yoon et al.[16] and consists of two groups of resonances, one at around 720 ppm and the other between 1350−1520 ppm, assigned to Li in Li layers (Li_{Li}) and in TM layers (Li_{TM}), respectively. (See Table 1 for a complete summary of notations used to describe the different sites for Ni and Li within the material.) The large shifts are caused by the hyperfine (Fermi contact) interaction.[31,32] A value for the concentration of the Li_{TM} ions of $9 \pm 2\%$ of the total Li content was determined by integration of the intensities of the different signals for the pristine spectrum, consistent with the number determined by ND.[18]

The resonance at 1520 ppm was assigned to Li_{TM} local environments near six Mn^{4+} ions in the first cation coordination shell ($LiMn_6$) and the resonance at 1350 ppm to environments containing five Mn^{4+} ions such as $LiMn_5Ni$.[16]

The Li_{TM} resonances have disappeared by 4.8 V, consistent with the fact that Li is removed from the TM layers.[16] The Li_{Li} resonance has shifted to lower frequency (around 530 ppm); this resonance is consistent with either Li in octahedral sites near diamagnetic ions such as Ni^{4+} or Li^{+} ions in tetrahedral sites, because both types of local environments are expected to result in a reduction of the Fermi contact shift.[32] The intensity of this resonance decreases noticeably when charging to 5.3 V, as Li atoms are deintercalated during the high-voltage electrochemical process. Deconvolution of the NMR spectra gives Li contents of 0.15 and 0.05 for the 4.8 V and the 5.3 V samples, respectively (assuming that the pristine material contains one Li, per formula unit), which is close (and within the error associated with the NMR measurements) to the respective values of 0.21 and 0.08 obtained from the specific capacity.

The intensity of the Li_{TM} resonance decreases after the first cycle between 4.6 and 2.0 V (Figure 4b), showing that only a fraction of the Li ions return to the Li_{TM} sites.

(31) Lee, Y. J.; Grey, C. P. *J. Phys. Chem. B* **2002**, *106*, 3576.
(32) Grey, C. P.; Dupré, N. *Chem. Rev.* **2004**, *104*, 4493.

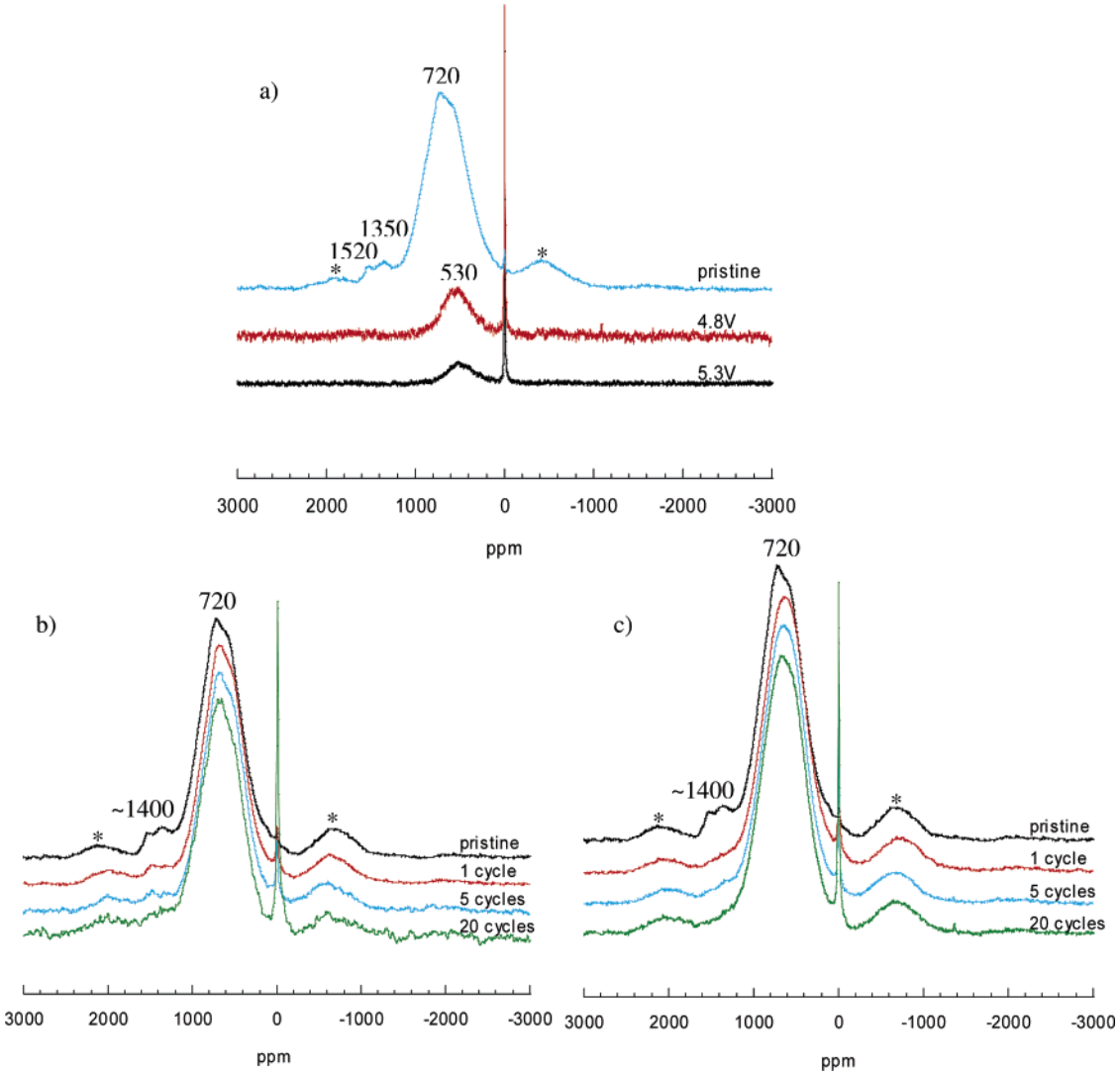

Figure 4. ^{6}Li MAS NMR spectra of (a) pristine $^6LiNi_{0.5}Mn_{0.5}O_2$ and $^6LiNi_{0.5}Mn_{0.5}O_2$ charged to 4.8 and to 5.3 V; (b−c) pristine $^6LiNi_{0.5}Mn_{0.5}O_2$ and the material cycled 1, 5, and 10 times, between 4.6 and 2.0 V (b) and between 5.3 and 2.0 V (c). The sharp resonance at 0 ppm arises from diamagnetic impurities ($LiPF_6$ in the electrolyte for instance). The major isotropic resonances and spinning sidebands are marked with their shifts and asterisks, respectively. Spectra were acquired at spinning frequencies of 38−40 kHz.

Table 1. Notations Used for This Study

symbol	description
Li_{Li}	lithium in lithium layer—octahedral site
Ni_{Li}	nickel in lithium layer—octahedral site
Ni_{TM}	nickel in the TM layer—octahedral site
Li_{TM}	lithium in the TM layer—octahedral site
Li_{TM}^{V}	vacated TM layer site formally occupied by Li—octahedral site
Ni_{TM}^{Li}	nickel that migrated to Li_{TM}^{V} site—octahedral site
Ni_{tet}	Ni in the tetrahedral site formed after removal of Li_{TM} and three Li_{Li} above
Li_{tet}	Li in the tetrahedral site formed after removal of Li_{TM} and three Li_{Li} above

However, this resonance is still clearly present, even after 20 cycles. In contrast, the Li_{TM} resonance has essentially disappeared after the first cycle between 5.3 and 2.0 V, the Li_{Li} resonance dominating the spectra (Figure 4c). Furthermore, a noticeable change in the Li_{Li} resonance is seen after only 1 cycle. The resonance becomes more symmetric, and the peak maximum shifts from 720 to 630 ppm. Only very small changes are seen in subsequent cycles. In contrast, the Li layer resonance changes only gradually following cycling between 4.6 and 2.0 V. The peak is still asymmetric even after 20 cycles. Li ions in the Li layers of Li_2MnO_3 give rise to two overlapping resonances at 700 and 750 ppm, due to local environments near four Mn^{4+} ions and two Li^+ ions in the TM layers; thus the disappearance of the higher frequency (720 ppm) component of the Li_{Li} line shape is consistent with the loss of Li_{TM} in these Li_2MnO_3-like environments. Thus the changes in the NMR spectra after cycling confirm that structural changes take place in the material and that these changes are accelerated by charging to 5.3 V.

ND. ND experiments of selected samples, prepared to investigate the effect of the high voltage plateau on electrode structure, were investigated. Rietveld[33] refinements of the structures were performed with GSAS-EXPGUI.[34] Because all the samples, except the pristine $^7LiNi_{0.5}Mn_{0.5}O_2$, contain graphite, two-phase refinements were performed, with $R\bar{3}m$ and $P6_3/mmc$ space groups for $^7Li_xNi_{0.5}Mn_{0.5}O_2$ and graphite,

(33) Rietveld, H. M. *J. Appl. Crystallogr.* **1969**, *2*, 65.
(34) Larson, A. C.; Von Dreele, R. B. *General Structure Analysis System (GSAS)*; Los Alamos National Laboratory Report LAUR 86-748; Los Alamos National Laboratory: Los Alamos, NM, 2000. Toby, B. H. *J. Appl. Crystallogr.* **2001**, *34*, 210.

Table 2. Rietveld Refinement Results for the ND Patterns[a]

	pristine	4.1 V	4.6 V	4.8 V	5.2 V	4.8−2.0 V	5.2−2.0 V
*x*Li	1	0.62	0.33	0.40	0.06	0.58	0.62
a (Å)	2.88226(4)	2.85575(8)	2.84499(5)	2.8488(1)	2.8431(3)	2.86914(8)	2.8818(1)
c (Å)	14.2619(4)	14.3846(8)	14.3104(5)	14.292(2)	14.047(3)	14.3313(9)	14.335(1)
V (Å^3)	102.606(3)	101.595(5)	100.309(3)	100.45(1)	98.33(1)	102.169(6)	103.10(1)
Ni_{Li} (3a; 0, 0, 0)	0.099(1)	0.115(2)	0.096(1)	0.042(2)	0.024(4)	0.060(2)	0.058(3)
Ni_{TM} (3b; 0, 0, 1/2)	0.401(1)	0.385(1)	0.404(1)	0.452(1)	0.476(4)	0.434(1)	0.405(3)
Ni_{tet} (6c; 1/3, 2/3, $z \approx 0.0456$)	0	0.000(2)	0.000(2)	0.006(2)	0	0.006(2)	0.038(2)
Li_{Li} (3a; 0, 0, 0)	0.901(1)	0.498(5)	0.212(5)	0.4	0.06	0.347(7)	0.58(1)
Li_{TM} (3b; 0, 0, 1/2)	0.099(1)	0.013(8)	0.016(5)	0	0	0.04	0.000(4)
Li_{tet} (6c; 1/3, 2/3, $z \approx 0.0456$)	0	0.120(4)	0.102(4)	0	0	0.194(6)	0.042(4)
z(O)	0.24160(3)	0.23740(6)	0.23617(5)	0.2373(1)	0.2395(2)	0.23828(6)	0.23801(9)
$100U_{iso}$ (Å^2)							
Li sites	2.60(5)	2.9(2)	4.2(3)	13.0(9)	0.7	6.1(3)	1.3(1)
Ni sites	0.60(1)	3.21(4)	2.43(3)	2.33(6)	1.14(8)	2.31(4)	2.30(6)
Mn sites	0.62(3)	3.6(1)	9.9(2)	2.4(1)	2.4(3)	2.3(1)	2.6(2)
O sites	1.00(1)	1.56(3)	0.58(2)	1.91(5)	2.17(9)	0.45(2)	0.63(1)
total R_{wp} (%)	5.81	2.49	4.42	3.06	4.27	4.35	2.78

[a] Cation occupancies (per formula unit $Li_xNi_{0.5}Mn_{0.5}O_2$), cation coordinates, and Wycoff symbols are given for the different crystallographic sites used in the refinement. A fixed occupancy of 0 was used if the refinement led to negative occupancy values. Parameters without standard deviations were constrained parameters.

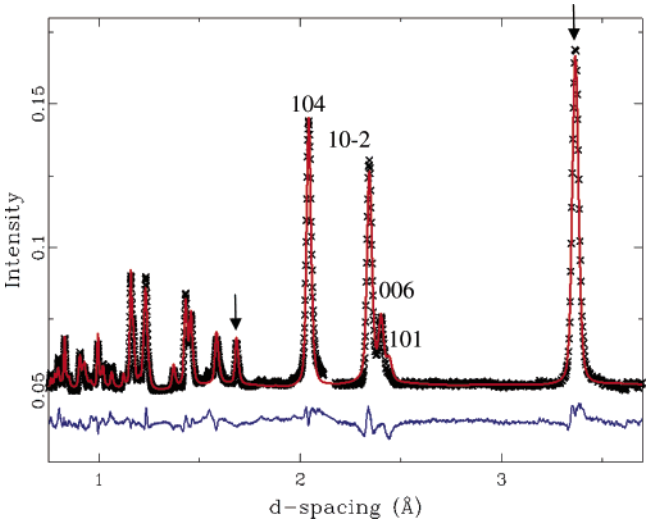

Figure 5. Rietveld refinement using the ND pattern (bank 4, from 50 to 75°, of the GEM detector) of $^7LiNi_{0.5}Mn_{0.5}O_2$ charged to 4.1 V. The crosses and the solid red line represent the experimental data and the calculated pattern, respectively. The difference between the calculated and experimental patterns is shown in blue below the data. The arrows show the reflections coming from graphite. The structural parameters are given in Table 2.

respectively. The structural parameters for the different ^7Li_x-$Ni_{0.5}Mn_{0.5}O_2$ samples are listed in Table 2. The Li contents *x* in these $^7Li_xNi_{0.5}Mn_{0.5}O_2$ electrodes were estimated from the capacity, by assuming 100% Coulombic efficiency, and these values were used in the refinements. These contents are consistent with ICP-OES measurements, which gave Li content values of 0.30, 0.14, and 0.63 (with an error of 10%) for the 4.8, 5.2, and 4.8−2.0 V samples, respectively. Figure 5 shows a representative neutron pattern from the series, for $^7LiNi_{0.5}Mn_{0.5}O_2$ charged to 4.1 V (where $x = 0.62$).

In previous structure refinements of the pristine material,[9,10] only Ni atoms, and not Mn atoms, were found in the lithium layer, due to the similar size of Ni^{2+} and Li^+ ions. Therefore, Ni/Li site exchange was allowed between the lithium and the TM layers for the pristine material, subject to a constraint that fixed the stoichiometry of the samples to the nominal Ni (0.5) and Li (*x*) concentrations. Given the highly correlated nature of refinements performed on systems with two atoms occupying the same sites, it was not possible to refine all the occupancies simultaneously. Instead, in the cycled samples, the Ni_{Li} and Li_{TM} site occupancies were first refined but were not constrained to be the same. Because Arachi et al.[22] observed Li and Ni occupancy in the tetrahedral sites, the fractions of Li and Ni in tetrahedral sites were also refined. This refinement procedure (first the TM sites and then the tetrahedral sites) was repeated at least three times until convergence. The refined occupancies are also shown in Table 2.

Given the very different scattering factors of ^7Li and Ni (−2.2 and 10.3, respectively[35]) and their opposite sign, the refinements were generally quite sensitive to small changes in cation occupancies. To assess this, refinements were performed where we varied Li/Ni contents systematically and examined the effect of this on *R* factors. In general, the tetrahedral sites were quite sensitive to changes in Ni occupancy. For example, a change in the Ni_{tet} site occupancy from 0.6% to 2.4% results in a significant change of R_{wp} from 4.35% to 4.46%, for the 4.8−2.0 V sample. For some samples, the occupancies of the octahedral sites were more highly correlated. In particular, the *R* factors for the refinement of the 4.8−2.0 V sample were particularly insensitive to large changes in the occupancies of the octahedral sites (see Supporting Information, Table S1). Hence, the Li occupancy of the TM layers was constrained to 0.04 in this sample, where this number was derived from an integration of an NMR spectrum of a material prepared in an analogous fashion (see Supporting Information, Figure S2). Once Li_{TM} is fixed, a change in the Li_{tet} content from 0.10 − 0.30, per formula unit $Li_xNi_{0.5}Mn_{0.5}O_2$, resulted in a change for Ni_{tet} of 0−0.024, and only a change of R_{wp} of 0.01% (Table S1), indicating that although the concentration of Li_{tet} ions is high (0.2 (±0.1) Li per formula unit), it is also associated with a large error; although the errors in the Ni_{tet} occupancy are similar, the concentration of this site is clearly low (>0.024). Unfortunately, the samples were radioactive following the

(35) Sears, V. F. *Neutron News 3* **1992**, *3*, 26.

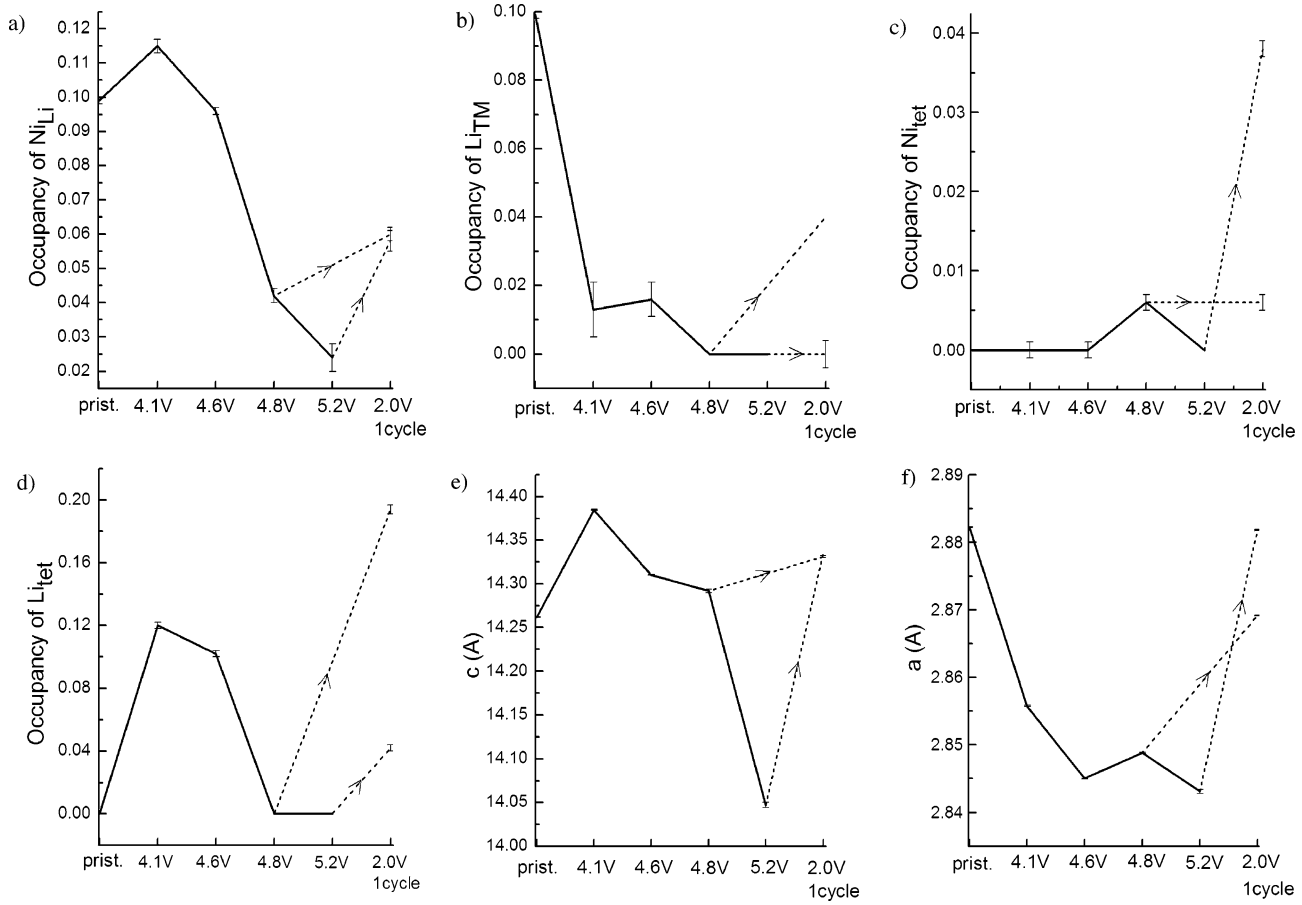

Figure 6. Evolution of parameters obtained from Rietveld refinements using ND data of pristine $^7LiNi_{0.5}Mn_{0.5}O_2$ and $^7LiNi_{0.5}Mn_{0.5}O_2$ charged to 4.1, 4.6, 4.8, and 5.2 V and cycled once between 4.8 or 5.2 and 2.0 V. The solid line and the dotted lines represent the first charge and discharge, respectively. Evolution of the fractional occupancy of (a) Ni in Li layers; (b) Li in TM layers; and (c and d) Ni and Li in tetrahedral sites, respectively. The error bars correspond to the maximum value of the standard errors obtained from Rietveld refinements. (e and f) Evolution of the *c* and *a* parameters, respectively.

ND experiments and joint X-ray−neutron experiments could not be performed on the same samples.

The fraction of both Li_{TM} ions decreases rapidly with increasing state of charge (Figure 6), while the Ni_{Li} occupancy drops noticeably only at high voltages. The Li_{TM} ions do not return to the TM layers if the sample is cycled between 5.2 and 2.0 V (Figure 6b), as confirmed by MAS NMR (Figure 4c), while a small fraction of the Ni_{Li} does return (Figure 6a). On the basis of this ND analysis, it is clear that noticeable structural changes do occur between 4.6 and 5.2 V. These changes are at least partially irreversible, as different cation occupancies are seen for the fully discharged samples following charging to 4.8 and 5.2 V. The Ni occupancy in the tetrahedral sites is very small throughout the charging process, while the Li occupancy in the tetrahedral sites reaches a maximum at half-charge. Both increase when cycled once between 5.2 and 2.0 V. The differences in the 4.6, 4.8, and 5.2 V samples are also apparent if the *a* and *c* parameters of these samples are considered (Figure 6e,f), the value of the *c* cell parameter decreasing dramatically from 4.8 to 5.2 V, indicating that the layers collapse upon further deintercalation of the remaining lithium atoms.

Because Arachi et al.[22] previously showed (by transmission electron microscopy and synchrotron XRD) that a second-order phase transition from hexagonal to monoclinic (*C*2/*m*) occurs during Li deintercalation of $Li(NiMn)_{0.5}O_2$, the refinements were also attempted with the *C*2/*m* space group. Patterns calculated with this space group contained additional reflections that were absent in our experimental patterns. Furthermore, no reductions in the *R* factors, over those observed with the space group $R\bar{3}m$, were observed. Our inability to detect a reduction in symmetry may be related to the higher resolution seen in synchrotron based experiments or slight differences in the samples.

In Situ XRD. In situ experiments were performed to follow the changes in cell parameters as a function of Li content. The changes in the *a* and *c* parameters (Supporting Information, Figure S5, and inset in Figure 10) seen upon charging to 4.8 V largely mirror those seen by ND, but in contrast to the ND results, the *a* and *c* parameters vary smoothly until full charge. These in situ results provide additional evidence that structural changes do occur above 4.6 V and that the capacity in this voltage range is not only due to side reactions involving the electrolyte.

First Principles Calculations. First principles calculations were performed to predict and rationalize the structural changes that occur on cycling. Three aspects were investigated in particular: (1) the thermodynamic driving force for Ni migration and the effect it has on the Li deintercalation voltage, (2) the activation barriers for Ni migration in the Li layer and toward the vacancies in the TM layer, and (3) the influence of interlayer spacing on the stability of Ni ions in the TM layers against migration into tetrahedral sites.

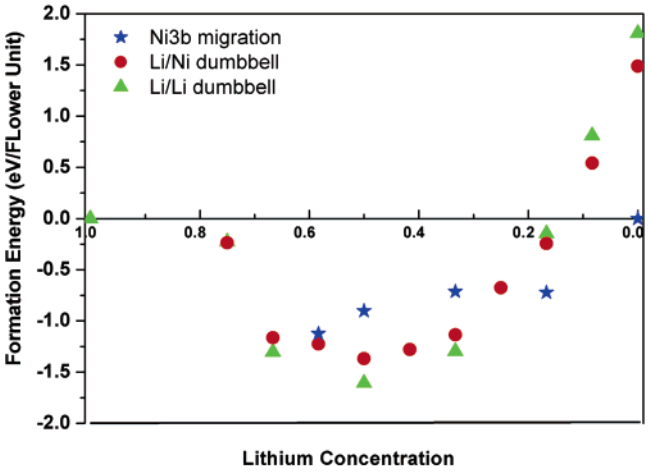

Figure 7. Formation energy as a function of Li concentration of structures with three different lithium/nickel configurations: no Ni_{Li} migration and formation of Li/Li dumbbells (triangles), migration of Ni_{Li} in tetrahedral sites to form Li/Ni dumbbells (circles), and migration of Ni_{Li} to fill Li_{TM}^{V} to become Ni_{TM}^{Li} (stars).

Computations require periodic supercells and, hence, an ordered arrangement of ions. These calculations were, therefore, performed using the previously proposed "flower" arrangement[19] with a supercell of 12 formula units (Figure 1c).

A. Ni and Li Rearrangements: Thermodynamic Driving Forces and Kinetic Barriers. To understand the thermodynamic driving forces acting upon the structure, we have calculated the energies of three types of structural modifications of the flower structure, as a function of Li composition: (1) Li extraction with no Ni migration, (2) Li extraction with migration of Ni from the Li layers, Ni_{Li}, into the tetrahedral sites, and (3) Li extraction with migration of Ni_{Li} into a vacant Li_{TM}^{V} site (in the TM layers; see Table 1) to become Ni_{TM}^{Li}. We later discuss whether such Ni migration is kinetically possible. The changes under scenario (1) were already presented in a previous paper,[19] and we include them here for completeness. Figure 7 shows the corresponding energies of $Li_x(Ni_{0.5}Mn_{0.5})O_2$ as a function of Li content. The quantity plotted is the energy difference between the mixed state and a compositionally averaged combination of $LiNi_{0.5}Mn_{0.5}O_2$ and $Ni_{0.5}Mn_{0.5}O_2$. Negative energies indicate that the intermediate compositions are stable, either as a solid solution, or as ordered states. Delithiation under scenario 1 (no Ni migration) involves the formation of Li/Li dumbbells (see Figure 2) around the Li_{TM}^{V} site in TM layers, vacated early in the charge process. These states (triangles in Figure 7) have the lowest energy at most Li compositions. Remarkably, the structural configuration in which Ni_{Li} migrates from the Li layer into the TM layer (scenario 3) has the lowest energy near the end of charge. The Li/Ni dumbbell configuration (formed from one Ni_{tet} and one Li_{tet} ion; Figure 2, scenario 2) is never lowest in energy for the well-ordered flower structure used for these calculations. However, the energy difference between tetrahedral Li/Ni and Li/Li dumbbells is very small (12−20 meV per $LiMO_2$ formula unit in the $x = 0.33-0.66$ range), and less favorable reference positions for Ni_{Li} in the pristine material (as would exist in a more disordered material) may lead to intermediate Li/Ni dumbbell formation. The energy difference between the Li/Li and the Li/Ni dumbbell can be rationalized on the basis of the oxidation states of the Ni ions. In this composition range, Ni_{Li} remains as 2+ and has a weak preference for octahedral coordination over tetrahedral coordination, according to ligand field theory.[36] Because of the way the flower ordering repeats along the *c* axis, dumbbell formation around every Li_{TM}^{V} results in occupied tetrahedra that share edges within one layer. As a result, the repulsion between Li^+/Ni^{2+} tetrahedra within the lithium slab space is stronger than that of Li^+/Li^+ tetrahedra and is responsible for their energy difference. Hence, it is to be expected that in more disordered materials than the one used in our computations, where some Ni_{Li} is in a higher energy state and more isolated Li/Ni dumbbells can form, some tetrahedral Ni will be present.

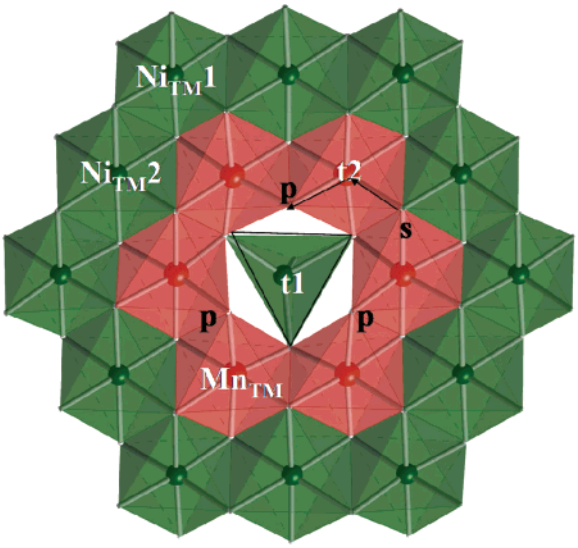

Figure 8. Schematics of different octahedral and tetrahedral sites in the flower structure; the tetrahedral t_1 site (green) is located above the vacant octahedral site in the flower structure Li_{TM}^{V}; Li_{TM}^{V} is surrounded by 6 Mn^{4+} (red) and then 12 more distant Ni^{2+} ions (green) in the TM layers. s, p, and t_2 are octahedral (s and p) and tetrahedral (t_2) sites in the Li layers.

More interestingly, the structural configuration in which Ni_{Li} has moved from the Li layer into the TM layer to fill the Li_{TM}^{V} site has the lowest energy near the end of charge, when the Li concentration is below 0.33. The driving force for this configuration is straightforward: when the last Li is removed, Ni_{Li} is oxidized to 4+. Such oxidation causes a large reduction in ionic size, and the Ni^{4+} strongly favors the TM site instead of the Li site. Nonetheless, the magnitude of this driving force (>1 eV per migrating Ni ion) is surprising. Tetrahedral site occupation by Ni is not favored in this composition region because the Ni^{4+} $3d^6$ electronic configuration strongly prefers octahedral coordination.

The energy results illustrated in Figure 7 indicate that there is a driving force for any Ni in the Li layer to migrate into the TM layer toward the end of charge. To investigate how readily this migration will occur, the kinetics of this process were studied. Figure 8 shows the relevant sites involved in the migration pathway. The central site in this figure is a Li_{TM}^{V} vacancy in the TM layer surrounded by Mn_{TM} and

(36) Figgis, B. N.; Hitchman, M. A. *Ligand Field Theory and its Applications*; Wiley-VCH: New York, **2000**.

Ni_{TM}. The lowest energy position for Ni_{Li} in this structure is the "s" site above the interface between the Mn_{TM} and the Ni_{TM} ring. The "p" site in the Li layers is closer to the Li_{TM}^{V} vacancy. For octahedral ions to diffuse in layered structures, the ions need to move through intermediate tetrahedral sites.[37] A Ni atom in the "p" site can easily slide into the tetrahedral site (t1) above the vacant Li_{TM}^{V} site. We found from computations that when a Ni^{2+} in the p site is oxidized to Ni^{4+} it spontaneously slides into the vacant Li_{TM}^{V} site without any activation barrier. If the Ni atom is further away from the vacancy in the TM layer, it will experience two factors that make its migration more difficult. The first factor is that when Li, Ni, and Mn atoms are well-ordered in a flower arrangement, the "s" site in the Li layer is the most stable one for Ni_{Li} and any migration away from this "s" site will require more energy.[18] Second and more importantly, for Ni in the s site to migrate to the p site, it needs to go through a tetrahedral site (marked as t2 in Figures 2 and 8), which shares a face with a Mn^{4+} octahedron. Ab initio computations previously showed the negative impact that a high-valent cation has on the activation barrier for Li migration, when that cation shares a face with the activated tetrahedral site.[15,37] Because of its higher charge, Ni^{2+} is even more affected by the charge on the face-sharing TM ion. Our calculations show that the energy barrier for Ni hopping between the s and the p site via t2 is as high as 1 eV/Ni. In the perfectly ordered flower structure, the Li_{TM} site is fully surrounded by six Mn atoms, and migration of Ni_{Li} into this site (after it has been vacated) will always require a high activation energy to cross the tetrahedral site t2 which face-shares with a Mn octahedral site. However, in less ordered materials, some $Li_{TM}-Ni_{TM}$ contacts are present,[18] which may create easier pathways for Ni_{Li} to migrate out of the Li layer. Hence, Ni migration from the Li layer into the TM layer may be easier in a more disordered material.

B. Effect of Ni Migration on Li Deintercalation Potentials. The potential depends strongly on which cation migrations occur during Li removal. Figure 9 shows the average calculated local voltage upon Li deintercalation under the three different structural evolution scenarios discussed in Figure 7. The voltage is calculated as the average in small concentration intervals (0.16 or 0.25 Li), and most steps are, therefore, artificial because the average voltage switches from one concentration interval to the other. Clearly, to obtain a more realistic voltage curve, many more possible Li/V configurations have to be explored.[29,38] A constant potential of between $x = 1$ and $x \sim 0.66$ is observed in experiments and corresponds to the simultaneous removal of Li_{TM} and some Li_{Li} as discussed previously.[19] The curve "Most stable" presents the voltages derived by taking the state with the lowest energy in Figure 9 for each composition. The only significant voltage difference between the various structural models occurs near the end of charge, for $x_{Li} < 0.33$. Removing the last 16.6% of lithium from the tetrahedral sites without any other configurational changes requires a potential as high as 5.2 V. It is slightly easier to extract Li from a Li/Ni dumbbell. In contrast, a significantly lower charge voltage is required if the oxidized Ni ions can migrate from the Li sites into the TM sites (squares). The potential predicted for this reaction (4.49 V) is remarkably close to the rest potentials for the cells charged up to 5.2 V seen in the OCV data (Figure 9). Our calculations suggest that at the end of charge Li removal is possible through two different processes: a fast process at very high potential that involves direct extraction of Li from tetrahedral sites and a lower voltage process that can only occur if the structure can relax through the migration of Ni ions. The former process does allow for removal of all Li from the material in "normal" voltage windows, which seems to be in agreement with the fact that the capacity in the first charge in most of our experiments approaches the theoretical limit.

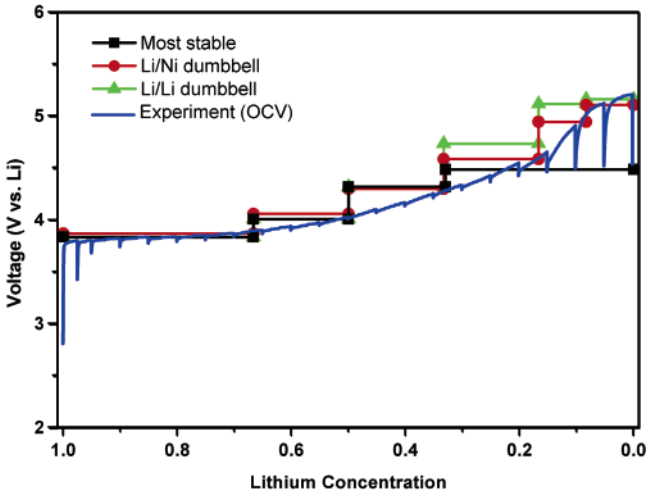

Figure 9. Comparison between the calculated voltage curves for different delithiation scenarios and the voltage profile during the first charge of a $Li/Li_x(NiMn)_{0.5}O_2$ cell charged to 5.3 V at 14 mA/g with intermittent OCV stands of 6 h. Experimental Li contents in $Li_x(NiMn)_{0.5}O_2$ were calculated assuming 100% Coulombic efficiency.

C. Effect of the Lattice Parameter on Dumbbell Formation. We have investigated to what extent these different structural scenarios affect the evolution of the *c*-lattice parameter. Although first principles DFT calculations within the LDA approximation systematically under-predict the lattice parameter, qualitative trends are often useful for comparison to experimental data (in situ XRD and ND). Figure 10 shows the *c*-lattice parameters from LDA+U calculations as a function of lithium concentration *x* under the three different scenarios previously described. Consistent with previous studies,[19] the formation of Li/Li dumbbells leads to a slight increase in the *c*-lattice parameter as Li is removed and the peak value of *c* appears at Li = 0.33. Between $x = 1$ and $x = 0.33$, the variation in the *c*-lattice parameter is small due to the presence of Ni in the lithium layer. The *c*-lattice parameter decreases upon further delithiation and at $x = 0$ is smaller by 4.4% over the lattice parameter in the pristine material. When some Li remains in the material, the contraction is much less (e.g., only −0.8% for $x = 0.167$). If Li/Ni dumbbells form during delithiation, the *c*-lattice parameter increases more significantly (+2.7%) and peaks at $x = 0.33$ as well. The contraction of *c* at the end of the charge is −5.8%. More importantly, Ni_{TM}^{Li} migration for *x*

(37) Van der Ven, A.; Ceder, G. *J. Power Sources* **2001**, *97*, 529.
(38) Arroyo y de Dompablo, M. E.; Ceder, G. *J. Power Sources* **2003**, *119*, 654.

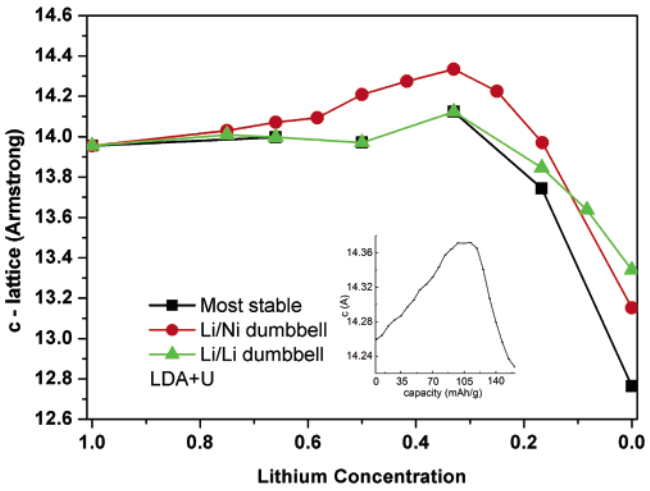

Figure 10. Calculated LDA+U *c*-lattice parameters as a function of Li concentration, with different structural scenarios. The inset shows the evolution of the *c* parameter obtained from Rietveld refinements using the in situ XRD patterns of $LiNi_{0.5}Mn_{0.5}O_2$, charged to 4.8 V.

< 0.33 causes the *c*-lattice parameter to collapse (−8.9%) upon complete charging.

Discussion

We now describe in more detail the reversible and irreversible structural changes that take place during charge and discharge.

Initial Stage of Deintercalation (up to 4.1 V; $x \approx 1.0$ to $x \approx 0.6$. The neutron data, NMR observations, and computations all indicate that Li is extracted from both the TM and the Li layers in the early stages of charge, consistent with observations made based on earlier NMR results[16] and computational modeling.[15] The ND data on the sample charged to 4.1 V confirms this picture. Only 0.01 Li remains in the TM layers (0.013 Li/per formula unit $Li_xMn_{0.5}Ni_{0.5}O_2$ for $x = 0.62$) on charging to 4.1 V, but a significant fraction now occupies the tetrahedral site (0.12 Li/per formula unit). If Li−Li dumbbells (Figure 2) are formed, the maximum number of tetrahedral Li ions is twice the amount originally present in the TM site in the pristine material. This is possible in the perfectly ordered flower, where there is perfect separation of the $LiMn_6$ rings and the Li/Li dumbbells are maximally separated. In a less well-ordered material, however, some of the adjacent, open tetrahedral sites will be too close together so that not all of them can be occupied. This seems to be the case in our samples. Diffraction results suggest that there are slightly less Li_{tet} (0.12 Li_{tet}) than predicted by the perfectly ordered flower model (0.172 Li_{tet}, based on the concentration of Li removed from the TM layers (0.086 Li)). The calculated structural energies (Figure 7) indicate that there are no significant driving forces for structural changes in this potential regime. Some migration of Ni^{2+} ions may occur in this regime, but this is barely significant. The fact that the Ni_{TM} occupancy drops slightly upon charge to 4.1 V (Table 2) may indicate that some Ni ions in high-energy TM sites have moved out of them (see later) or may simply be the result of the limitations inherent in the structural refinements.

Charging between 4.1 and 4.6 V ($x \approx 0.6$ to $x \approx 0.3$). Between 4.1 and 4.6 V (to $x = 0.33$), Li is largely extracted from the Li layers, the residual concentration of Li ions in the TM layers remaining constant. No change is seen in the concentration of Li_{tet}, further confirming that all tetrahedral Li forms early in the charge process and no configurational changes that would create additional sites for tetrahedral Li (i.e., by moving Ni_{Li}) take place. Our results are quite different from those of Arachi et al.,[22] who have investigated the structure of $Li_xNi_{0.5}Mn_{0.5}O_2$ on charging to a composition of $x = 0.33$, by using synchrotron XRD. Their $x = 0.6$ and 0.4 samples contain 0.4 and 0.3 Li_{tet} per formula unit, respectively, and 0 and 0.02 Ni_{tet}. The occupancies of these tetrahedral sites are higher than twice the concentration of vacancies in the TM layers seen in our work, implying very short Li_{tet}−TM contacts. No TM vacancies are seen in their work. We note, however, that Li occupancies are quite difficult to determine with any accuracy in disordered systems by using X-ray based methods, due to the low scattering factor of Li. Their trends in *a* and *c* parameters are similar to ours over the same composition range suggesting that the samples are similar.

Charging to 5.2 V ($x \approx 0.3$ to $x \approx 0$). The Li NMR and diffraction results clearly indicate that structural changes in $LiNi_{0.5}Mn_{0.5}O_2$ take place on charging to high potential, leading to an almost fully delithiated material. ND results in combination with the earlier work by Seel and Dahn[30] indicate that PF_6^- insertion in graphite accounts for at least some of the capacity seen at higher voltages. However, as discussed in detail in Supporting Information, this process will contribute only 3.0−4.5 mAh g^{-1}, which is much smaller than the capacity observed at high voltages. Between 4.6 and 5.2 V all the Li ions in the tetrahedral and TM layers are removed, leaving only a few residual Li_{Li} ions at 5.2 V ($x = 0.06$). Li NMR confirms that all the Li_{TM} is removed by 4.8 V and that Li_{Li} sites are removed from 4.8 to 5.2 V. Given our uncertainty in the 4.8 V sample prepared for ND, it is difficult to be certain when the Li_{tet} is removed in this range. The concentration of Ni_{tet} is barely significant in this range. The Ni_{Li} concentration decreases noticeably in this voltage window, dropping from 0.1 Ni at 4.6 V to only 0.02 Ni at 5.2 V. Consistent with the energetic driving force shown by the first principles computations, we speculate that this is due to the Ni_{Li} ions migrating into the TM sites. While the measured *c*-lattice parameter drops at 5.2 V, its relative decrease is not as much as in the first principles computations (Figure 10). The calculated *c*-lattice parameter is very sensitive to the amount of ions in the interslab space in this compositional range, and the difference between calculation and experiment is likely due to the fact that the Ni migration is only partial in the experimental sample consistent with the smaller changes in lattice parameters.

We believe that the limiting factor for the Ni_{Li} to Ni_{TM} migration process is the oxidation of Ni in the Li site. This site is larger than the TM site, and hence the oxidation to 4+ will only occur for Ni_{Li} after most of the Ni_{TM} is oxidized.[39] Some preliminary first principles computations (not shown) have confirmed this oxidation sequence. The structural energies in Figure 7 clearly support this picture.

(39) Peres, J. P.; Delmas, C.; Rougier, A.; Broussely, M.; Perton, F.; Biensan, P.; Willmann, P. *J. Phys. Chem. Solids* **1996**, *57* (6−8), 1057.

Until the end of charge is near and Ni_{Li} becomes oxidized, there is no energetic benefit for moving the Ni ions, even though vacancies exist in the TM layer. Hence, it is not so much the Li content that controls the Ni migration but rather the Ni oxidation state. Of course, in a stoichiometric sample such as $LiNi_{0.5}Mn_{0.5}O_2$ these two are coupled, but the distinction may be relevant for materials where the Ni content is lower (and hence oxidation of Ni_{Li} would be reached earlier). Our kinetic results indicate that there may be two distinct time scales for this Ni migration: Ni_{Li} that is close to the tetrahedral site above the TM vacancy moves into the TM vacancy without a barrier as soon as it is oxidized (probably around 4.6 V), while a Ni_{Li} ion that needs to diffuse over a $LiMn_6$ ring has a substantial activation barrier. It is interesting to note that while charging potentials of 5.2 V are required to remove the last Li ions, the rest potential in this regime is much closer to 4.5 V (Figure 9). Comparing these numbers to the calculated results (Figure 9) would indicate that the high potential is required to remove the tetrahedral Li ions but that, at rest, the structure relaxes by migrating some Ni ions from Li to TM sites, thereby bringing the potential down to ≈4.5 V. It is likely that this slow process corresponds to the Ni ions that have to diffuse across well-ordered $LiMn_6$ rings.

Discharge Process. The refinement on the discharged sample (down to 2.0 V) indicates that the migration of Ni from the Li to the TM sites is not permanent. Upon discharge the concentration of Ni_{TM} almost returns back to its pristine value. In particular, upon discharge from 5.2 V about 0.07 Ni ions (per formula unit) have disappeared from the TM site. Of this 0.07 Ni, about 0.03 returns back to the Li site and 0.04 now occupies the tetrahedral site. Given that the relative stability between Ni in Li and TM layers depends on its oxidation state, this is not surprising. Upon reduction to 2+, Ni again prefers the Li site. Using first principles computations we have investigated in somewhat more detail the energetics and kinetics of the process whereby Ni returns to the Li layer and find that the driving force for Ni to move out of the TM layer depends on its environment. Figure 11 shows the energy to migrate Ni from various environments in the TM layer at a Li concentration $x = 0.67$. Configuration **A** is the one that is likely formed at the end of charge. It corresponds to the flower structure with the center of the flower occupied by Ni (instead of Li in the pristine material). As shown in Figure 11, this type of Ni ion, surrounded by six Mn^{4+} ions, is the least stable and may lower its energy by moving into the tetrahedral site in the Li layer to form a Li/Ni dumbbell (configuration **B**). Configuration **C** corresponds to **A** but with a Ni_{TM} ion that was surrounded by four Mn^{4+} ions moved into a tetrahedral site. Clearly, there is no driving force to move this Ni ion into the tetrahedral site. An even higher energy increase is found when a Ni at the edge between flowers (surrounded by three Mn^{4+}) migrates to a tetrahedral site. There is a consistent trend showing that Ni surrounded by more Mn^{4+} ions is more unstable in the octahedral site in the TM layer, indicating simple electrostatic reasons for this variation in stability. Because NMR shows that Li_{TM} in the pristine material is preferentially surrounded by six Mn^{4+}, some of the Ni^{4+} ions

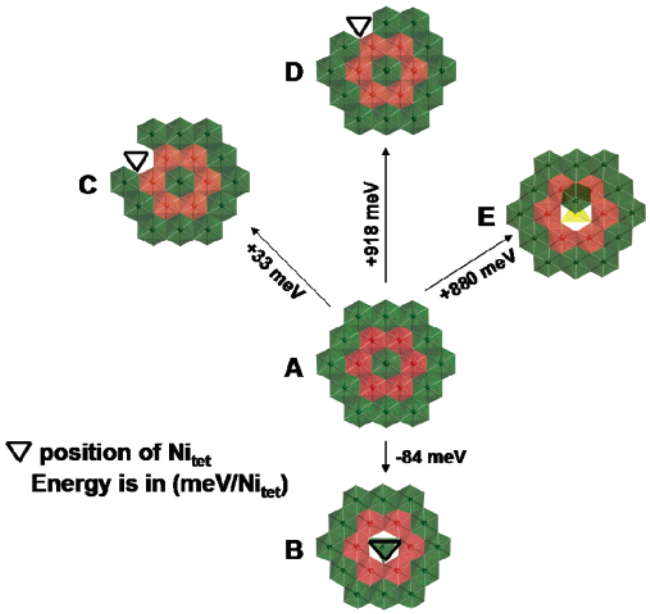

Figure 11. Energy change when different Ni_{TM}^{Li} migrate to tetrahedral sites or Li layers. (A) Ni_{TM} surrounded by six Mn^{4+} (no tetrahedral occupancy of Li), (B) Ni_{TM} moves to Ni_{tet} forming a Li/Ni dumbbell, (C) Ni_{TM1} surrounded by four Mn^{4+} moves to Ni_{tet} forming Li/Ni dumbbell, (D) Ni_{TM2} surrounded by three Mn^{4+} moves to Ni_{tet} forming a Li/Ni dumbbell, and (E) Ni_{TM}^{Li} moves back to Ni_{Li}. All migrations (B−E) are accompanied by Li_{tet} formation. The calculations were performed at a lithium concentration of 0.66. One (or zero) dumbbell is formed per 12 formula units.

that migrate at the top of charge into these sites may actually come out again. Ni ions that have moved into TM sites that are surrounded by five Mn^{4+} and one Ni^{2+} are less likely to come out based on the first principles data. (Evidence for this environment comes from the NMR spectra of the pristine material, where the resonance at 1350 ppm was assigned to Li near five Mn^{4+} and one Ni^{2+}). This may explain why the concentration of Ni ions in octahedral sites of the Li layers increases again upon discharge but does not return to its original value. Hence, a dynamical migration of Ni ions in and out of the TM layers takes place upon charging and discharging of this material. After discharge some Ni is present in the tetrahedral sites. This tetrahedral Ni likely arises from the Ni that migrates out of $NiMn_6$ TM environments but cannot diffuse further into Li sites, possibly because of the high activation barrier across this ring or because some of the Li sites are already re-filled with Li.

Ni Motion. Ni_{Li} hopping within the lithium layer is energetically difficult, according to first principles calculations, because the energy barrier is as high as 1 eV/Ni. Hence, both *the location* of the Ni_{Li} in the Li layers and *the redox state* of the Ni_{Li} are critical factors that appear to control Ni motion during charge/discharge and the exact Li concentration where Ni migration may happen. If Ni_{Li} does reside in one of the three p-type sites shown in Figure 8 at Li =1, two scenarios can happen. Either a Ni_{tet} site may be occupied upon charge (Li ∼ 0.58 or lower) and form a Li/Ni dumbbell or, because both Ni^{3+} and Ni^{4+} have a strong preference for octahedral coordination,[32] if Ni_{Li} is oxidized to 3+/4+ before migrating to a tetrahedral site, it becomes immobile. This may explain why Ni_{Li} never drops to 0% in the ND refinements. From the first principles computation, Ni_{Li} must

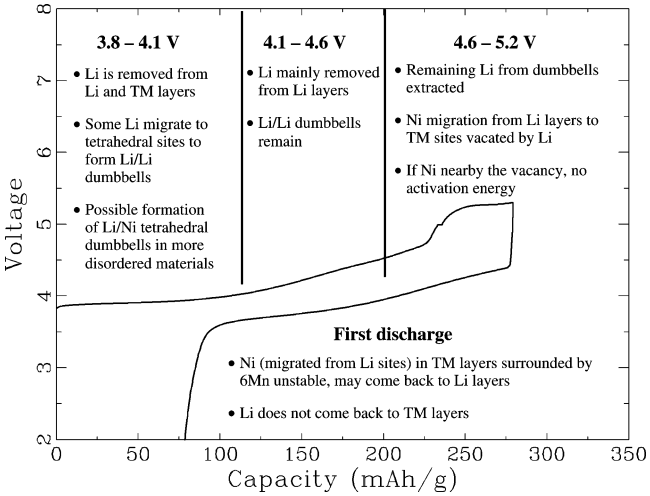

Figure 12. Summary of structural changes during the first cycle between 5.3 and 2.0 V.

be 4+ to be energetically favorable to move to the TM layer. Therefore, Ni_{TM}^{Li} migration is only expected at very high potential (low Li concentration 0.33 to 0).

Importance of the State of Order in the Material on the Structural Evolution. The computational results show that a well-ordered flower structure is least likely to reduce its Li/Ni exchange with cycling, for a number of reasons. The most stable site for Ni in the Li layer is away from the vacant Li_{TM}^{V} site that it needs to occupy. Diffusion of this Ni requires a hop through a tetrahedral site that face-shares with a Mn^{4+} octahedron. Such a hop has a very high activation barrier.[15] But most importantly, the site that Ni can occupy in the TM layer is surrounded by six Mn^{4+} ions, which we find to be the least stable at the Ni_{TM}^{Li} site. Hence, even if this Ni migrates to the TM layer, it is also most likely to come back out upon discharge. In less ordered materials, not all Li_{TM} is surrounded by six Mn^{4+} ions, and $LiMn_5Ni$ and $LiMn_4Ni_2$ exist,[18] as seen by NMR and in our simulations of the partially disordered state (Figure 1d). Such a lack of perfect $LiMn_6$ rings will give Ni_{Li} better access to the vacancy in the TM layer and lead to a more stable site once the Ni has migrated there. This may be one reason why in general quenched samples of $LiNi_{0.5}Mn_{0.5}O_2$ (less well-ordered) show better electrochemical properties than samples that are slowly cooled or annealed.[40]

Conclusions

Experimental data and first principles calculations clearly show that the structural changes that occur on cycling $Li(NiMn)_{0.5}O_2$ synthesized via the hydroxide route are complex. This complexity is due largely to the Li/Ni exchange that occurs between the Li and the TM layers in this predominantly layered compound. The presence of Li in the TM layer plays a strong role in controlling cation ordering in this layer, which then impacts the structural changes that occur on cycling. These structural changes are summarized in Figure 12.

(40) Meng, Y. S.; Kumar, S.; Hinuma, Y.; Bréger, J.; Kang, K.; Grey, C. P.; Shao-Horn, Y.; Ceder, G. **2006**, manuscript in preparation.

Charging to above 4.6 V results in the removal of essentially all the Li ions and the migration of approximately 75% of the Ni_{Li} into the sites in the TM layers vacated by Li. The ease of Ni migration depends on a large number of sometimes interrelated factors, but the Ni_{Li} oxidation state is critical. Only when Ni_{Li} is oxidized to 4+, at the very end of charge, do calculations show that there is a substantial driving force (>1 eV) to move into the vacancy in the TM layer. The migration energy on discharge strongly depends on the Ni environments in the TM layers, and environments where the Ni ions are surrounded by six Mn^{4+} ions are unstable. While in the current material the Li content and Ni^{4+} content are clearly correlated, the results suggest that it may be possible to optimize the Ni^{2+} content of a material independently so as to minimize or control the extent of Ni migration.

There appear to be (at least) two different time scales for Ni migration which depend on the distance between Ni in the Li layers and the vacancies in the TM layers. Long-range Ni migration involves (at least) one hop via a tetrahedral site that shares a face with a highly charged TM ion, which is associated with a large activation energy. The computational results are consistent with the electrochemical results, where the Ni migration/Li loss process is seen at above 5.0 V for experiments performed in galvanostatic mode, while the OCV data reveal a process at 4.5 V. Taken together, all the data indicate that the Ni migrations will occur even for materials charged to only 4.6 V, but the process will occur much more slowly and over a number of cycles.

The results have wider implications for other related materials, because they suggest that similar Ni migrations can occur if certain conditions are met. For example, Ni migration and structural rearrangements may occur more readily upon charging in the materials $Li[Li_{1/3-2y}Mn_{2/3-y}Ni_y]O_2$ in samples that have been prepared by quenching, rather than by slow cooling, because the latter samples are typically more well-ordered and contain more Li ions in the TM layers surrounded by six Mn^{4+} ions. Conversely, structural rearrangements may be minimized for the sample of $Li[MnNi]_{0.5}O_2$ prepared via the sodium form,[15] by using samples in which environments where Ni^{2+} is surrounded by five or more Mn^{4+} ions are minimized. Finally, it is remarkable that even with the dynamic Ni rearrangements at every charge and discharge cycle there is little or no capacity fading in these materials, even when cycled to high potentials. This indicates that some structural changes to the Li host, even those involving diffusive processes, are acceptable for reversible intercalation.

Acknowledgment. The work was supported by the Assistant Secretary for Energy Efficiency and Renewable Energy, Office of FreedomCAR and Vehicle Technologies of the U.S. DOE under Contract No. DE-AC03-76SF00098, via subcontracts No. 6517748 and 6517749 with the Lawrence Berkeley National Laboratory. We would also like to acknowledge the support form the Center for Materials Science and Engineering, MIT, and the MRSEC program of the NSF under award number DMR 02-13282. Y.S.-H. acknowledges the Office of Naval Research Young Investigator Award No. N00014-03-10448 for financial support. The ISIS Facility of the Rutherford Appleton Labora-

tory is thanked for access to GEM. This work has benefited from the use of NPDF at the Lujan Center at the Los Alamos Neutron Science Center, funded by the DOE Office of Basic Energy Sciences (BES), Los Alamos National Laboratory, and the DOE under Contract No. W-7405-ENG-36. The upgrade of NPDF has been funded by NSF through Grant DMR 00-76488. This work has benefited from the use of the Intense Pulsed Neutron Source at Argonne National Laboratory. This facility is funded by the U.S. DOE under Contract No. W-31-109-ENG-38. Use of the NSLS, Brookhaven National Laboratory, was supported by the U.S. DOE, Office of BES, under Contract No. DE-AC02-98CH10886. We are grateful for the assistance given to us at the different beam lines from Thomas Proffen (NPDF, LANL), Winfried Kockelmann (GEM, ISIS), Yongjae Lee (X7A, NSLS), James Richardson, Evan Maxey, and Ashfia Huq (GPPD, IPNS). We thank Jordi Cabana for electrochemical measurements as well as Matthias Gutmann and Alan Soper for their help in neutron data analysis.

Supporting Information Available: Voltage vs specific capacity curves for $LiNi_{0.5}Mn_{0.5}O_2$ used for ND and in situ XRD experiments, and $LiNi_{0.5}Mn_{0.5}O_2$, table showing the sensitivity of the refinement to the Li occupancy of the tetraheral site for the 4.8−2.0 V sample, ^{6}Li MAS NMR spectrum of $^6Li_xNi_{0.5}Mn_{0.5}O_2$ cycled between 4.8 and 2.0 V, calculation of the capacity associated with PF_6^- intercalation in graphite, ND data, and evolution of the *a* parameter using the in situ XRD patterns of $LiNi_{0.5}Mn_{0.5}O_2$ (PDF). This material is available via the Internet at http://pubs.acs.org.

CM060886R